Potential Vortex Transient Analysis and Experiment

John R. Cipolla

Email: john@aerorocket.com

709 West Homeway Loop, Citrus Springs FL 34434

Abstract

A series of experiments and hydrodynamic analyses has been conducted to resolve the paradox that a viscous-flow distribution between concentric cylinders can be identical to a potential vortex (inviscid-flow) distribution at steady state. Where a potential vortex or tornado can be described as the flow around and through a drain hole at the bottom of a large container. As an approximation to this phenomenon, an experimental device to simulate a three dimensional potential vortex was fabricated that used a rapidly rotating central cylinder or rotating core located on the axis of a cylindrical basin filled with water. The fluid surface shape and velocity profile of an artificially generated potential vortex or free vortex was experimentally measured and compared with hydrodynamic models to define the viscid and inviscid nature of the potential vortex flow. A new program called VORTEX based on a finite difference solution of the Navier-Stokes equations was developed to determine the transient velocity profile and transient free surface shape of the potential vortex for comparison with experiment. From these experiments it is proposed the paradox is resolved because energy-momentum is conserved in a potential vortex under steady state conditions. This work can be applied to the measurement of the potential vortex flow generated by aircraft wing tips, interior flow of aircraft jet engines, rocket motor propellant tanks and natural phenomena like tornadoes, hurricanes and General Relativity.

Nomenclature

a_n = Centripetal acceleration

CFL = Non-dimensional stability criterion

E = Kinetic energy

g = Acceleration of gravity

M = Mass

p = Static pressure

p_{atm} = Atmospheric pressure

r = Radial coordinate

r_0 = Radius of the inner cylinder

r_1 = Radius of the outer cylinder

t = Time coordinate

T_{ss} = Time to reach steady state

u_θ = Circumferential fluid velocity

u_r = Radial fluid velocity

U = Potential energy

V_0 = Surface velocity of the inner cylinder

W = Weight of an object

W_f = Friction losses

W_s = Mechanical work

z_1 = Height of fluid at maximum radius

z_0 = Vertical intersection of free surface and rotating cylinder

z_{0s} = Still height of fluid

Greek symbols

Δr = Radial increment

Δt = Time increment

θ = Circumferential coordinate

ω = Rate of angular rotation (Hz)

μ = Coefficient of viscosity

ρ = Fluid density

ν = Kinematic viscosity (μ/ρ)

ω_z = Fluid vorticity

I. Introduction

An experimental device to simulate a three dimensional potential vortex was fabricated that used a rapidly rotating central cylinder or core located on the axis of a cylindrical basin filled with water. One purpose of this paper is to document the difficulty of fabricating an experiment to generate a "standing" potential vortex without the inherent mechanical vibrations that can cause turbulence in the flow field and make physical measurement difficult. For even a well-designed apparatus, physical measurement of the potential vortex surface is extremely difficult because of the constant wave action caused by turbulence and flow separation. At first it was envisioned that a probe extended onto the surface might be used to indicate surface location relative to a datum surface like the still height, z_{0s}. Where, the still height is the fluid surface location in the basin when the rotating core is stationary. Instead, for comparison of theoretical and experimental fluid surface shapes and velocity profiles the following approaches were used. First, theoretical surface shapes are superimposed on photographs of the corresponding observed surface shapes for a graphical approach to data reduction. Second, physical measurement of fluid velocity was only practical in the center of the basin where turbulence effects were not significant. Physical measurement of free surface velocity in the central location of the basin was achieved by using video that recorded the motion of a small Styrofoam ball placed in the vortex to determine orbital velocity of the fluid carrying the ball. Also, this paper proves the velocity profile equation for a potential vortex where the outer cylinder is located infinitely far away is not sufficient to model the case of fluid flow between two concentric cylinders. Instead, an analysis where the inner cylinder rotates and the outer cylinder is stationary is required to accurately model the velocity profile. Finally, an attempt is made to explain why the transient flow between two concentric cylinders used to generate a potential vortex has a steady state viscous-flow velocity distribution that is identical to inviscid potential-flow.

II. Potential Vortex Experiment

A. Description.

To validate the potential vortex solution based on the continuity, momentum and energy equations an experiment was fabricated using two concentric cylinders, an inner cylinder rotating at velocity V_0 and a stationary outer cylinder. The two concentric cylinders are separated by a distance represented by the ratio, $r_1/r_0 = 5$ where r_1 is the radius of the outer cylinder and r_0 is the radius of the inner cylinder.

FIG 1. Experiment with central cylinder rotating at 15 Hz.

The first element and the most critical feature of the experimental apparatus designed to create a potential vortex to simulate the phenomenon of water flowing down a drain consists of a rapidly rotating Plexiglas cylinder with an outside diameter of 3.35 cm and overall length of 20.8 cm. The centrally positioned Plexiglas cylinder uses two sealed bulkheads to support a one-piece aluminum drive shaft that is approximately 30.0 cm long and supported at the bottom end by a brass bearing and at the motor drive end by another brass bearing that simply centers the shaft while the shaft is being driven by the motor using a drive-pin that connects the motor and drive shaft. The single drive-pin allows the rapidly rotating shaft to float in the brass bearing assembly without excessive vibration or side-to-side interference with the top brass bearing assembly. The second element of the vortex generator consists of a stationary Plexiglas cylinder or basin that

forms the outer boundary of the flow field which has an inside diameter of 16.4 cm and overall height of 23.6 cm. A DC motor speed control and small DC motor form the third element of the vortex generator. Rotation speed of 2 to 30 cycles per second (Hz) is possible using the system depicted in Figure 1. Finally, the rotation rate measurement system illustrated in Figure 1 forms the forth and final element of the vortex generator. The measurement system consists of a standard bicycle speed measurement computer, magnetic probe and a drum attached to the shaft that holds the sensor magnet. As displayed in Figure 1 the velocity of the rotating drum is 4.6 km per hour, which means the rotating drum holding the sensor magnet has a rotation rate of 15 Hz. This is the rotation rate of the shaft and the rotating cylinder when driven by the DC electric motor.

B. Experimental and theoretical free surface deflection compared

A potential vortex or tornado is often approximated by the flow around a drain hole at the bottom of a container. As an approximation to this phenomenon and to generate a standing vortex, an experimental device to simulate a three dimensional potential vortex has been fabricated that uses a rapidly rotating central cylinder located on the axis of a cylindrical basin filled with water. A rotating cylindrical core forms the inner boundary around which the potential vortex is created while maintaining an approximately non-viscous or inviscid boundary condition on the outer boundary of the flow. The rotating inner boundary's non-slip or viscous boundary drags circumferential layers of fluid that generate the potential vortex. The rotating inner core of the experiment represents the rotating inner boundary of the potential vortex. The circumferential velocity profile for the potential vortex at steady state is:

$$u_\theta = \frac{V_0 \ r_0}{r} \tag{1}$$

Where r is measured from the center of the system, V_0 is the rotation velocity at the surface of the inner vortex core and r_0 represents the radius of the inner rotating cylinder. Velocity in the radial direction, u_r is zero and r_1 represents the outer radius of the stationary cylindrical basin. Figure 2 displays the geometry for the free surface and velocity profile analysis and provides nomenclature for the experiment. During initial startup, viscous interactions between subsequent layers of fluid generate a time varying velocity profile and free surface deflection. The transient phase of flow cannot be

considered irrotational. However, at steady state the velocity profile and free surface deflection of the resulting fluid flow can be approximated by an irrotational solution based on the viscous Navier Stokes equations in the circumferential, radial, and vertical (θ, r, z) directions when the proper boundary conditions are imposed. The Navier Stokes solution for the potential vortex generates a velocity distribution that is incompressible where $\nabla \cdot V = 0$ and irrotational where $\nabla \times V = 0$ throughout the flow field at steady state. The final solution for the steady state potential vortex is the Bernoulli equation, that holds everywhere in the flow including the free surface where $p = p_{atm}$ and forms a series of constant-pressure surfaces having the form of a second-order hyperboloid, that is, z varies inversely with r^2. Where the Bernoulli equation for p is expressed as[1].

$$p = \frac{\rho\,K^2}{2\,r^2} + \rho\,g\,z = C \tag{2}$$
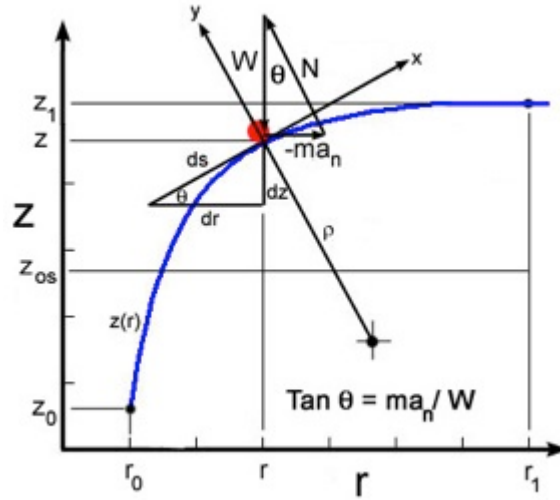
FIG. 2. Free body diagram for an object on the free surface of a potential vortex.

Where $K = V_0\,r_0$ and the constant, C must be determined to compute the shape of the fluid surface at $p = p_{atm}$ which represents the free surface of the potential vortex described in Figure 2. After solving for fluid height, z using the Bernoulli equation, then applying the pressure boundary condition $p = p_{atm}$ on the free surface to determine the constant C, a free surface of constant pressure p_{atm} has the following shape as a function of r from the center of the rotating cylinder.

$$z_{p=p1} = C_1 - \frac{V_0{}^2 r_0{}^2}{2\,g\,r^2}. \text{ Where } C_1 = z_0 + \frac{V_0{}^2}{2g} \tag{3}$$

Then, Eqn. 3 can be rearranged with one unknown, z_0 remaining.

$$z = z_0 + \frac{V_0^2}{2g}\left(1 - \frac{r_0^2}{r^2}\right) \tag{4}$$

Where, z_0 is the vertical intersection of the fluid free surface with the central rotating cylinder from the bottom of the basin illustrated in Figure 2. The unknown distance is determined by solving the following fluid volume equation.

$$VOL_{total} = VOL + VOL' \tag{5}$$

Where VOL_{total} is the total, still or motionless volume of fluid when the initial depth of the fluid in the basin is z_{0s}, VOL is the volume of fluid below the plane defined by $z = z_0$ and the bottom of the basin and VOL' is the volume of fluid determined by integrating between the free surface (Eqn. 4) defined by $p = p_{atm}$ and plane $z = z_0$. The following three equations define the three fluid volumes required to determine the unknown.

$$VOL_{total} = \pi(r_1^2 - r_0^2)z_{0s} \tag{6}$$

$$VOL = \pi(r_1^2 - r_0^2)z_0 \tag{7}$$

$$VOL' = \frac{\pi V_0^2}{2g}\left\{(r_1^2 - r_0^2) - 2r_0^2\ln\frac{r_1}{r_0}\right\} \tag{8}$$

Finally, after some algebra the resulting equation for the vertical intersection of the fluid free surface with the central rotating cylinder from the bottom of the basin becomes.

$$z_0 = z_{0s} - \frac{V_0^2}{2g}\left\{1 - \frac{2r_0^2}{(r_1^2 - r_0^2)}\ln\frac{r_1}{r_0}\right\} \tag{9}$$

The potential flow equations represented by Eqn. 4 and Eqn. 9 are used to produce the surface deflection curves superimposed on the experimental shapes depicted in Figures 3-4 for rotation rates of 10 Hz and 15 Hz respectively. Results in Figure 3 validated the experimental free surface deflection by superimposing theoretical surface deflection on a photographic image of the actual surface deflection. Table I displays potential vortex surface measurement results compared to theoretical inviscid and irrotational potential vortex flow. Measurement of the potential vortex surface was extremely difficult because of the constant wave action superimposed on the surface. At first it was envisioned that a probe extended onto the surface might be used to indicate surface location relative to a datum surface like the still height, z_{0s}. The still height is the fluid surface location in the basin when the central core is stationary. Instead, for comparison of theoretical and experimental fluid surface deflection the following approach was used.
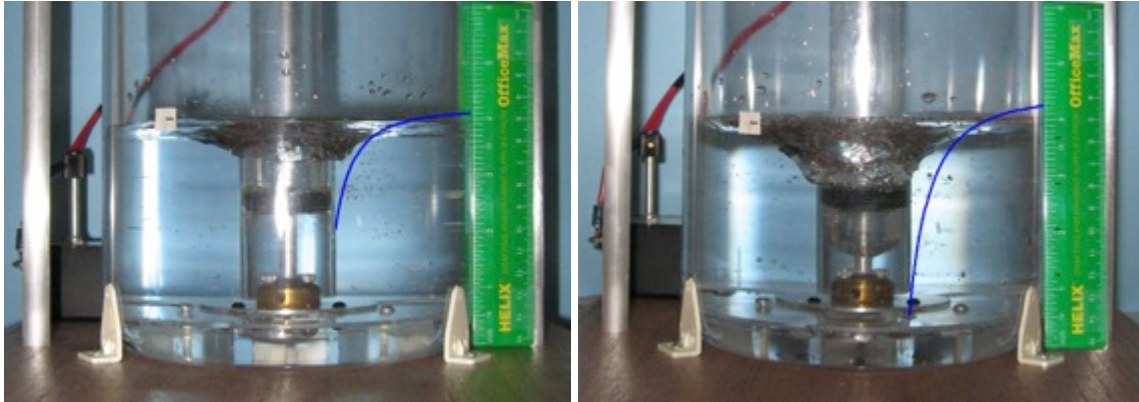
FIG. 3. Experimental free surface and theoretical free surface compared. (a) 10 Hz, (b) 15 Hz
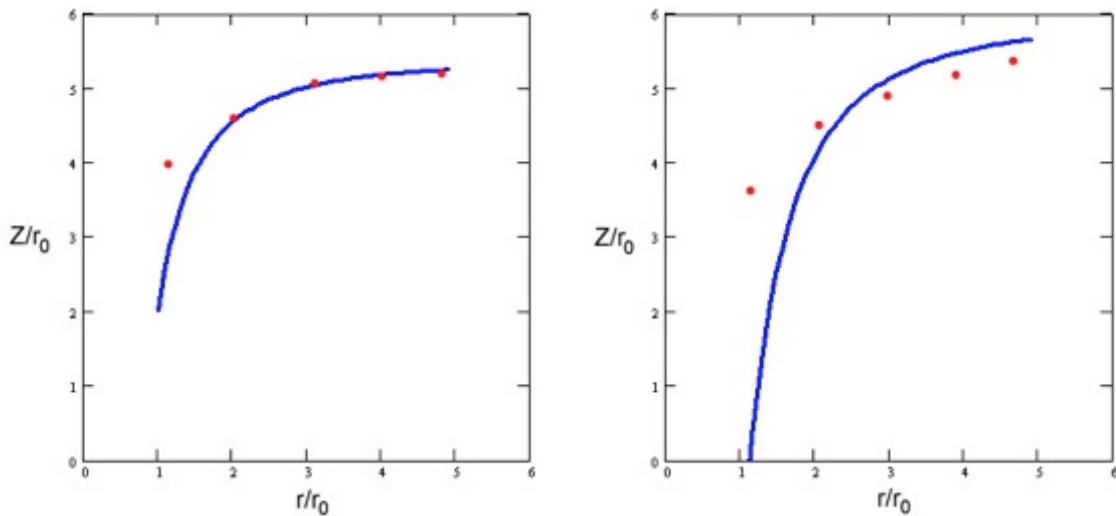
FIG. 4. Experimental (red dots) verses theoretical (blue line) potential vortex surfaces. (a) 10 Hz, (b) 15 Hz

As illustrated in Figure 3a and Figure 3b theoretical potential vortex surface shapes are superimposed on photographs of the corresponding experimental surface shapes for a graphical approach to data reduction. When generating the composite images displayed in Figures 3-4 care was taken to properly scale the curves using marks on the theoretical plots and marks on the images of the fluid vortex rotating at 10 Hz and 15 Hz. In Figures 3-4 please note that agreement between experimental and theoretical surface shapes is best for the 10 Hz case because turbulence effects are less than for the corresponding 15 Hz case. In both cases agreement between theoretical and experimental results were worse near the rotating cylinder due to intense turbulence and flow separation. However, agreement between experimental and theoretical surface shapes based on Eqn. 4 is good.

TABLE I. Summary of theoretical verses measured potential vortex surface deflection.

ω_0 Hz	z_{0s}(cm) Still height From bottom	z(cm) $r = 3.5\ cm$ Equation 4	z(cm) $r = 3.5\ cm$ **Measured**	$z_1(cm)$ $r = r_1$ Equation 4	z_1(cm) $r = r_1$ **Measured**
10	8.26	7.77	7.2 (-7.33%)	8.80	8.4 (-4.54%)
15	8.26	7.17	6.7 (-6.55%)	9.48	8.7 (-8.23%)

Free surface shape measurements are displayed in Table I when the central cylinder rotates at 10 Hz and 15 Hz. The values displayed in the second, third and fifth columns are theoretical potential vortex deflections measured from the bottom of the basin where $z = 0$. As noted by these measurements good agreement between theoretical and experimental free surface deflection is achieved in the central region of the potential vortex because turbulence effects are minimal. In contrast, the region near the rotating core departs from potential vortex theory due to intense turbulence caused by flow separation from the surface of the rotating core.

C. Experimental and theoretical free surface orbital velocity compared

Potential vortex surface velocity is determined by measuring the time it takes a red-spotted Styrofoam ball to orbit the potential vortex by using a video camera to document the orbital motion on the surface of the potential vortex. Physical measurement of free surface fluid velocity was only practical in the center of the basin where turbulence effects were not significant. Measurement of free surface velocity was achieved by using video that recorded the motion of a Styrofoam ball placed in the vortex to determine orbital velocity of the fluid carrying the ball knowing the radius and orbital period.

The following discussion describes how the orbital velocity of an object on the free surface relates to surface velocity of a potential vortex. The local surface shape of a potential vortex that supports an orbiting object, allows an object to orbit at a velocity that is a function of core rotation rate, radius to the object on the free surface and free surface curvature or inclination. The velocity of an object on the free surface is due to the dynamic equilibrium between object inertia, ma_n object weight, W and the local surface

deformation or curvature of the free surface. Specifically, the local slope of the vortex free surface under an orbiting object allows the object to be in dynamic equilibrium under the action of its own weight, W normal force, N exerted by the surface and the inertia vector, $-ma_n$ directed opposite to a_n.

FIG. 5. Free surface rotation velocity experiment

FIG. 6. Free surface rotation velocity movie. Requires **QuickTime**.

Where, the centripetal acceleration, a_n is directed away from the center of the circular path of the object when the object is in orbit around the rotating core of the vortex. The local deformation or curvature of the vortex free surface causes the object to orbit in the direction of rotation of the inner surface. Therefore, the velocity of the object orbiting at a point on the free surface is purely a function of the physical characteristics of the inner

surface having some angular rate of rotation and radius. This analysis implies local curvature of a potential vortex allows the object to orbit on the surface and objects placed on the surface move at the same orbital velocity as the potential vortex in those locations. Also, orbital velocity of an object on the potential vortex is derivable from the curvature or slope of the free surface and is identical to the potential vortex velocity specified by Eqn. 1. For this experiment, free surface velocity was validated using video that recorded the motion of a small Styrofoam ball placed in the vortex to determine orbital velocity of the fluid carrying the ball. Then, after selecting a segment of the video when the ball is at the center of the basin an accurate fluid surface rotational velocity can be calculated by measuring the time of rotation from the video. The data displayed in Figure 7a and Figure 7b indicates the presence of the stationary outer cylinder significantly affects the velocity profile correlation between theory and experiment. A solution of the continuity and momentum equations verified the cylinder separation has a profound effect on the velocity profile as illustrated in Figures 7a and Figure 7b but correlation between experiment and theory has been achieved to within engineering accuracy.
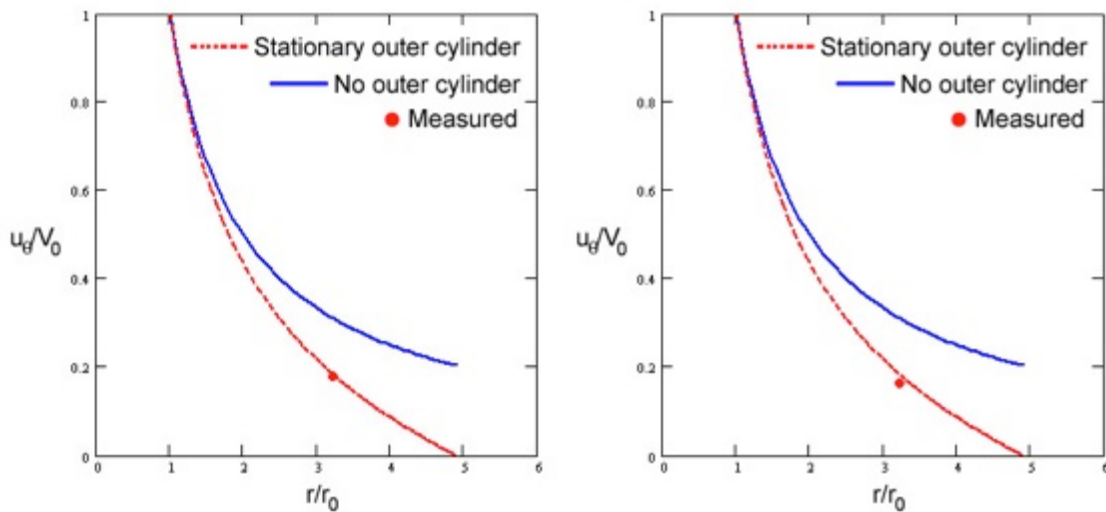
FIG. 7. Potential vortex velocity profile compared to theoretical prediction. (a) 10 Hz, (b) 15 Hz

Figure 7a and Figure 7b present results of the experiment where *No outer cylinder* represents the case where there is no outer cylinder and *Stationary outer cylinder* represents the case where the outer cylinder is a finite distance away. For the 10 Hz rotation rate the orbital radius was determined from the video to be 5.4 cm from the

center of the basin and the time to orbit the basin was 1.8 seconds. Additionally, for the 15 Hz rotation rate the orbital radius was also determined to be 5.4 cm from the center of the basin and the time to orbit the basin was 1.3 seconds. The surface velocity results displayed in Table II are within engineering accuracy indicating the analysis for the *Stationary outer cylinder* where the outer cylinder is a finite distance away is valid. In addition, only when the outer cylinder is located infinitely far away does the velocity profile result in true irrotational potential vortex flow as depicted by the curve labeled N*o outer cylinder* (Eqn. 1). This experiment generated potential vortex flow that is nearly irrotational because the data labeled *Measured* compares favorably to the theoretical analysis represented by the curve labeled, *Stationary outer cylinder* (Eqn. 23) for the cylinder separation used in this experiment. However, designing an experiment that generates true irrotational potential vortex flow would require a r_1/r_0 ratio so large that the cost would be prohibitive. Therefore, for the generation of a nearly irrotational potential vortex the separation ratio $r_1/r_0 = 5$ used in this experiment is considered sufficient[12]. However, the objective here was to design an experiment that is capable of producing a fluid flow having the theoretical properties of a potential vortex in the region away from the concentric walls.

TABLE II. Summary of theoretical verses measured potential vortex surface velocity at R_{orbit}.

ω_0 (Hz)	V_0 (cm/sec)	r_0 (cm)	R_{orbit} (cm)	T_{orbit} (sec)	$\dfrac{u_{\theta\_orbit}}{V_0}$ Eqn. 1	$\dfrac{u_{\theta\_orbit}}{V_0}$ Eqn. 23	$\dfrac{u_{\theta\_orbit}}{V_0}$ **Measured**
10	105.2	1.675	5.4	1.8	0.31	0.183	0.179 (-2.2%)
15	157.9	1.675	5.4	1.3	0.31	0.183	0.165 (-9.8%)

III. Verifying that potential vortex flow is irrotational

Potential vortex irrotationality was determined by observing the axial rotation rate of a red-spotted ball while orbiting the potential vortex. To determine the sense of rotation of a point on the vortex free surface a 2.22 cm diameter red-spotted ball was inserted on the surface when the flow was fully developed at steady state. The orbiting ball experiment, as illustrated by the QuickTime movie in Figure 8, indicates potential vortex flow is

irrotational when the vortex is fully developed at steady state because the ball does not rotate around its vertical axis relative to the surface of the potential vortex. However, when the central core is turned off the flow is rotational because the ball rotates around its vertical axis during the coast phase to zero motion.
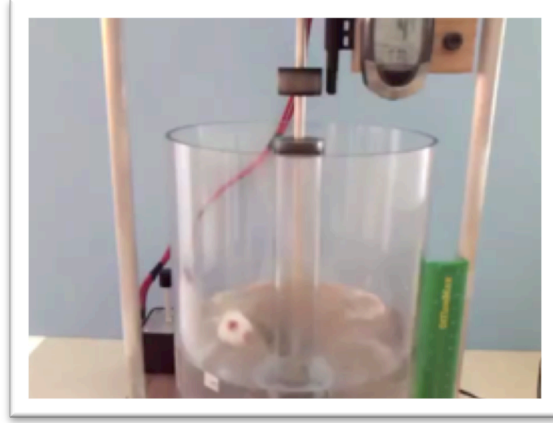
FIG. 8. Free surface velocity and ball-spin movie. Requires **QuickTime**.

The following analysis illustrates that for potential vortex flow or the flow outside a rotating central core, the flow is irrotational because vorticity, ω_z is zero. This experiment illustrates the flow is irrotational because the red spotted ball moves as a solid body in the central region of the basin. The vorticity of potential vortex flow is computed as follows. Where, the angular motion of a particle is defined as $\omega_z = \frac{1}{2}\nabla \times \boldsymbol{V}$.

$$u_\theta = \frac{V_0 r_0}{r} \tag{10}$$

$$V_0 = r_0\omega. \text{ Therefore } u_\theta = \frac{r_0^2 \omega}{r} \tag{11}$$

$$\omega_z = \frac{1}{r}\frac{\partial(ru_\theta)}{\partial r} - \frac{1}{r}\frac{\partial u_r}{\partial \theta} \tag{12}$$

$$\omega_z = 0 \tag{13}$$

In addition, for a solid vortex or the region within a rotating central core, the fluid flow is rotational because vorticity is non-zero. The vorticity of solid vortex flow is computed as follows. Where, the angular motion of a particle is defined as $\omega_z = \frac{1}{2}\nabla \times \boldsymbol{V}$.

$$u_\theta = r\omega \tag{14}$$

$$\omega_z = \frac{1}{r}\frac{\partial(ru_\theta)}{\partial r} - \frac{1}{r}\frac{\partial u_r}{\partial \theta} \tag{15}$$

$$\omega_z = 2\omega \tag{16}$$

By definition, ω_z is defined as the net angular rotation that measures the localized spin of a fluid particle along its path of travel. As a consequence if $\omega_z = 0$ the flow is irrotational and the vorticity, $\nabla \times V$ must be zero. However, if the flow is rotational then the vorticity $\nabla \times V$ must be non-zero for a fluid particle along its path of travel. This definition indicates the free surface carrying the red spotted ball at the central point where the rotation was observed is irrotational and frictionless for potential vortex motion.

IV. General case of flow between two concentric cylinders

The following is a general derivation of the velocity profile between two concentric cylinders where viscous effects have been neglected. The continuity and momentum equations and the associated boundary conditions for the flow field between rotating concentric cylinders[3, 4] is presented for the case of a central rotational solid vortex and outer irrotational potential vortex. These equations prove that a rotational solid vortex is at the heart of every potential vortex, which follows naturally from fluid mechanics.

Continuity:

$$\frac{\partial u}{\partial \theta} = 0 \tag{17}$$

r momentum:

$$\frac{dp}{dr} = \frac{\rho u_\theta^2}{r} \tag{18}$$

θ momentum:

$$\frac{d^2 u_\theta}{dr^2} + \frac{d}{dr}\left(\frac{u_\theta}{r}\right) = 0 \tag{19}$$

The fluid boundary conditions at the inner cylinder, r_0 and the outer cylinder, r_1 can be specified as the following.

$$r = r_0: u_\theta = r_0 \omega_0, p = p_0 \text{ and at } r = r_1: u_\theta = r_1 \omega_1 \tag{20}$$

The solution for u_θ can be put in dimensionless form as the following.

$$\frac{u_\theta}{r_0 \omega_0} = \frac{r/r_0}{r_1^2/r_0^2 - 1}\left(\frac{\omega_1 r_1^2}{\omega_0 r_0^2} - 1\right) - \frac{r_0/r}{\left(1 - r_0^2/r_1^2\right)}\left(\frac{\omega_1}{\omega_2} - 1\right) \tag{21}$$

The velocity profile in the limit where the inner cylinder vanishes ($r_0 = 0$) and the outer cylinder rotates at rotation rate, ω_1 represents the case of rotational solid-body rotation.

$$u_\theta = \omega_1 r \tag{22}$$

Finally, the following equation is used to generate the red-dashed curve in Figures 7a and Figure 7b labeled *Stationary outer cylinder*, where the data point *Measured* is the result of this experiment. This equation generates the velocity profile in the θ direction when the inner cylinder rotates and the outer cylinder is stationary. The following equation provided the best fit with measured surface velocity displayed in Figure 7.

$$u_\theta = \frac{r_0 \omega_0}{r_1^2 / r_0^2 - 1} \left(\frac{r_1^2}{r_0 r} - \frac{r}{r_0} \right) \tag{23}$$

In the limit as the outer cylinder is placed infinitely far away ($r_1 \to \infty$) the flow becomes a true potential vortex of the familiar form presented previously.

$$u_\theta = \frac{r_0^2 \omega_0}{r} \tag{24}$$

In terms of rotating inner cylinder strength, K the velocity profile for a potential vortex is the following. Where $K = V_0 r_0$.

$$u_\theta = \frac{K}{r} \tag{25}$$

V. Transient velocity solution[4, 6, 8] using the Navier-Stokes equation

Steady state flow between two concentric cylinders is inviscid and irrotational when the inner cylinder rotates and the outer cylinder is stationary. However, during the transient or startup phase the flow is viscous and governed by the Navier-Stokes equations in cylindrical coordinates where u_r, u_θ and u_z are flow velocities in the r, θ and z directions respectively. To prove the paradox that transient free vortex flow is viscous and the steady state solution is inviscid and irrotational the following analysis using a finite difference solution of the Navier-Stokes equations in cylindrical coordinates is presented. For this application a CFD computer code called VORTEX was developed to model the general response of transient viscous flow between concentric cylinders. For one-dimensional viscous flow the velocity is only a function of θ, t and viscosity. Therefore, the Navier-Stokes equations reduce to the following single equation.

$$\mu \left[\frac{\partial^2 u_\theta}{\partial r^2} + \frac{1}{r} \frac{\partial u_\theta}{\partial r} - \frac{u_\theta}{r^2} \right] = \rho \frac{\partial u_\theta}{\partial t} \tag{26}$$

After central differencing Eqn. 26 the resulting time marching finite difference equation to determine velocity distribution as a function of time takes the following form.

$$u_n^{t+1} = u_n^t + \text{CFL} \left[\left(1 + \frac{\Delta r}{2 r_n} \right) u_{n+1}^t - \left(2 + \left\{ \frac{\Delta r}{r_n} \right\}^2 \right) u_n^t + \left(1 - \frac{\Delta r}{r_n} \right) u_{n-1}^t \right] \tag{27}$$

Where the non-dimensional time and stability criterion in Eqn. 27 is defined as follows.

$$\text{CFL} = \frac{\mu}{\rho} \frac{\Delta t}{(\Delta r)^2} \tag{28}$$

For these equations μ represents the coefficient of viscosity, ρ is the fluid density, Δt is the time increment and Δr is the special increment in the radial direction of fluid flow. Table III summarizes numerical and stability criteria for the VORTEX finite difference numerical analysis using Eqn. 27 and Eqn. 28. Where, adjusted viscosity allows the transient solution to reach steady state (T_{ss}) in 2.46 minutes compared to 2.7 minutes for the experimentally observed steady state response of the potential vortex free surface.

TABLE III. Numerical analysis input parameters and kinematic viscosity.

CFL	r_0(cm)	r_1(cm)	z_{0s} (cm)	N	$\nu = \frac{\mu}{\rho} \left(\frac{m^2}{sec} \right)$	T_{ss} (Minutes)
0.5	1.675	8.2	8.26	50	1.05E-6 (water)	2.7 (measured)
0.5	1.675	8.2	8.26	50	1.05E-5 (adjusted)	2.46 (analysis)

Boundary conditions on the interior and exterior of the flow field determine if the solution represents the case where the outer stationary cylinder is located infinitely far away as represented by Eqn. 24 or if the outer cylinder is located a finite distance away as represented by Eqn. 23. The boundary conditions on the interior and exterior of the flow are represented by the following relationships. First, for when the outer cylinder is located infinitely far away (Eqn. 24).

$$u_{r=r_1} = u_{r=r_{N-1}} \tag{29}$$

Then, for when the outer cylinder is located a finite distance away (Eqn. 23).

$$u_{r=r_1} = 0 \tag{30}$$

For both cases the velocity boundary condition on the inner cylinder is as usual.

$$u_{r=r_0} = V_0 \tag{31}$$

The finite difference solution of the Navier-Stokes equation predicts the flow between two concentric cylinders is viscous and rotational during the transient or time-dependent phase. However, at steady state the results are exactly equivalent to the potential flow equations represented by Eqn. 23 and Eqn. 24 where the flow is inviscid.
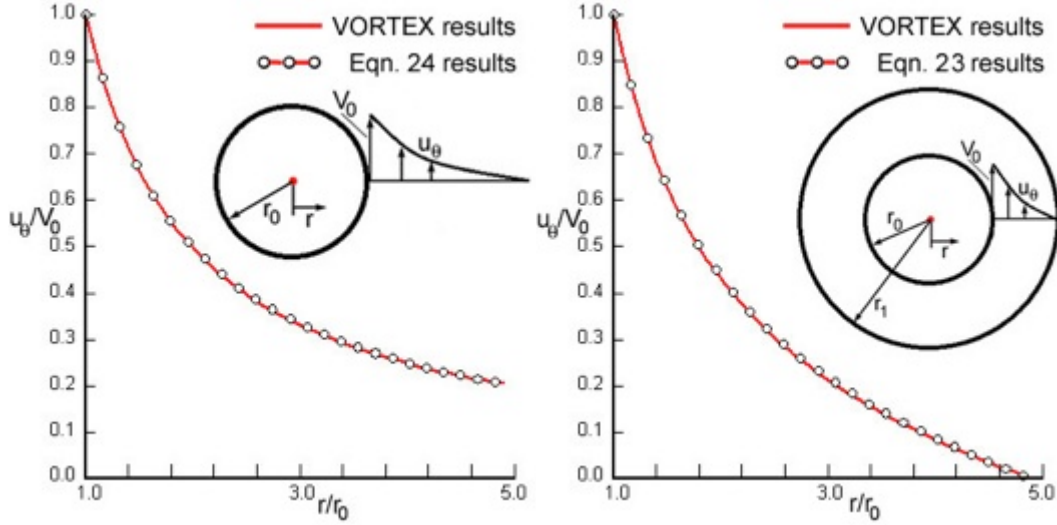
FIG. 9. Velocity profile. (a) Infinitely far apart (3000 iterations). (b) Finite distance apart (1750 iterations).

Solution of the Navier-Stokes equation (Eqn. 27) using the finite difference approach is illustrated in Figure 9a and Figure 9b. These results prove that during the transient phase of fluid motion the flow is viscous and rotational but at steady state the flow is irrotational and can be modeled using irrotational methods of fluid dynamics like the Bernoulli equation (Eqn. 2). In Figure 9 the steady state solution is derived from a transient analysis using a finite difference approximation to the Navier-Stokes equation and the boundary conditions specified by Eqns. 29-31. Figure 9a plots VORTEX velocity profile verses potential vortex theory when the outer cylinder is infinitely far away. Figure 9b plots VORTEX velocity profile verses potential vortex theory when the outer cylinder is a finite distance away. Convergence to steady state required 3000 iterations when the outer cylinder is located infinitely far away and 1750 iterations when the outer cylinder is located a finite distance away. Convergence required a stability criterion equal to 0.5 as specified by Eqn. 28. Results displayed in Figure 9 explain why the measured free surface velocity plotted in Figure 7a and Figure 7b agree better with the concentric cylinder predictions labeled *Stationary outer cylinder* for both the 10 Hz and 15 Hz rotation cases. As stated previously, the presence of an outer cylinder greatly affects potential vortex velocity. However, these results also show that surface shape predicted by Eqn. 4 is reasonably accurate for cases where the cylinder is located infinitely far

away or a finite distance away. However, accuracy departs greatly from measurement near the rotating cylinder where turbulence and flow separation are most intense.

VI. Transient free surface shape

Using methods available the only technique that accurately defines potential vortex steady state is the measurement of transient free surface shape. Therefore, program VORTEX free surface transient shape theory and analysis is developed. Free surface shape as a function of time requires the free vortex transient velocity profile[5, 6] derived previously starting from the Navier-Stokes equations. Transient height of the free vortex fluid surface measured from the bottom of the basin is determined by starting with the fluid height equation (Eqn. 4) which was derived from Bernoulli's equation and then inserting the following equation for y to normalize, r.

$$y = \frac{r}{r_0} \tag{32}$$

The resulting equation for potential vortex fluid height at steady state is the following.

$$g(z - z_0) = \frac{V_0{}^2}{2}\left(1 - \frac{1}{y^2}\right) \tag{33}$$

It is possible to prove algebraically that by using Eqn. 33 the time-dependent velocity profile determines the free surface transient height and therefore shape measured from z_0. The following integration provides the transient free surface shape for a potential vortex that is the generalized form of Eqn. 33 using a time-dependent velocity profile.

$$z - z_0 = \frac{V_0{}^2}{g} \int_1^{y_1} \left(\frac{u_\theta}{V_0}\right)^2 \frac{dy}{y} \tag{34}$$

The transient height of fluid above the plane $z = z_0$ is determined from the volume equation (Eqn. 5) where VOL', the transient volume of fluid above the plane $z = z_0$, is determined by the following integration.

$$VOL' = 2\pi \int_1^y r\, dr\, dz \tag{35}$$

Then, z_0 the location of the intersection of the fluid surface with the inner rotating cylinder is determined using the volume equation (Eqn. 5).

$$z_0 = z_{0s} - \frac{2}{(r_1{}^2 - r_0{}^2)} \int_1^{y_1} r\, dr\, dz \tag{36}$$

Finally, the general solution for the transient height of the fluid surface from the bottom of the basin can be determined from available information. The following equation for the time-dependent (transient) shape of the fluid surface is used in VORTEX.

$$z = (z - z_0) + z_0 \qquad (37)$$
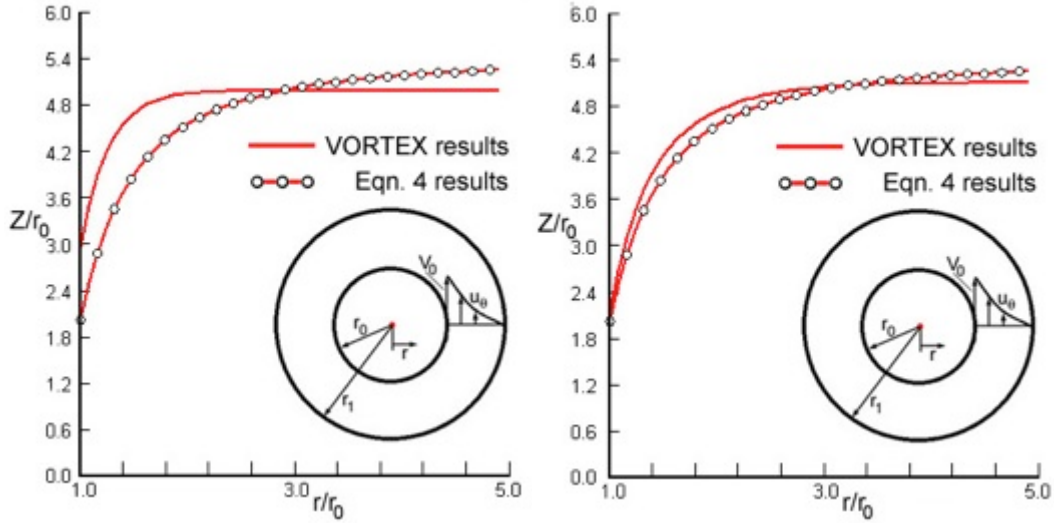
FIG. 10. Transient surface at 10Hz, cylinders finite distance apart. (a) 150 iterations. (b) 1750 iterations.

Figure 10a and Figure 10b prove the transient response of the fluid surface is captured by program VORTEX and that the fluid free surface develops with time to achieve a steady state condition. Experimentally observed free surface shape is used to determine the time required (T_{ss}) to a achieve steady state condition. Steady state is defined as the point in time when no discernable change occurs in free surface height on the outer stationary cylinder. The experimentally determined time to achieve steady state was approximately 2.7 minutes. However, VORTEX predicted a T_{ss} of approximately 24.64 minutes using the kinematic viscosity for water. Where, the standard value of kinematic viscosity (v) for water is $1.05E - 6 \ m^2/sec$. However, for the T_{ss} predicted by VORTEX to match experiment, kinematic viscosity required an order of magnitude reduction. The transient analysis results provided in Table IV illustrates that by reducing kinematic viscosity of water good theoretical agreement is achieved for the steady state time, T_{ss}. Having to reduce kinematic viscosity for the experimental and theoretical correlation of T_{ss} clearly illustrates that turbulent conditions around the rotating cylinder are accelerating the rate

of momentum transfer into the fluid and that steady state conditions are affected by the conservation of energy and momentum into the fluid. Reynolds number (R_e) displayed in Table IV clearly illustrates the flow surrounding the rotating cylinder is turbulent. Where, for the 10 Hz and 15 Hz rotation rates the Reynolds numbers are 35,081 and 52,622 respectively and the reference length is the diameter of the rotating cylinder, $D_{ref} = 2r_0$. Reynolds number greater than the transition value of 2,000 indicate the flow is turbulent; greatly accelerating the time it takes to achieve steady state.

TABLE IV. Transient solution results using adjusted kinematic viscosity (ν) for steady state time.

ω_0 Hz	T_{ss} (Minutes) **Measured**	R_e	z(cm) $r = 3.5\ cm$ VORTEX	z(cm) $r = 3.5\ cm$ **Measured**	z_1(cm) $r = r_1$ VORTEX	z_1(cm) $r = r_1$ **Measured**
10	2.7	35,081	8.06	7.2 (-11.9%)	8.55	8.4 (-1.79%)
15	2.7	52,622	7.82	6.7 (-16.7)	8.92	8.7 (-2.53%)

In conclusion, the viscous-flow distribution for a free vortex is identical to the potential-flow distribution at steady state because the energy-momentum into a fluid volume equals the energy-momentum out of a fluid volume balancing the viscous effects of fluid motion. This relationship is shown in the Bernoulli equation (Eqn. 2) where the first term on the right represents kinetic energy (E) and the second term on the right represents gravitational potential energy (U). The kinetic energy of potential vortex flow (Eqns. 23-24) and the gravitational potential energy of fluid displaced above the still height is balanced by the work performed by the viscous boundary layer at the surface of the rotating cylinder. The mechanical work performed by the viscous fluid is represented by the following equation[7]. Where, τ is the shear stress ($newton/m^2$) acting on the rotating cylinder and on the opposite side of each differential volume of fluid.

$$W_s = \int_{\theta_i}^{\theta_f} \tau\, d\theta \tag{38}$$

This result is a statement of the work-kinetic energy theorem[5] where mechanical work is performed by the rotating inner boundary. For the Bernoulli equation (Eqn. 2) the units for work, kinetic energy and potential energy is $joules/m^3$. The energy equation[1] takes the following simplified form during the startup phase of rotating cylinder motion.

$$W_s + W_f = \Delta(p + E + U) \qquad (39)$$

Finally, it should be noted that for the case where the outer cylinder is infinitely far away it would take an infinite amount of time for Eqn. 24 to transfer enough momentum (ρu_θ) for the fluid system to attain a steady state velocity profile[3]. Therefore, the viscous-flow distribution is identical to the potential flow distribution at steady state because work performed by the rotating cylinder (W_s) compensates for viscous losses (W_f) in the fluid.

VII. Conclusions

The results of this experimental and analytical analysis of potential vortex flow demonstrate that at steady state it is relatively simple to measure the free surface shape and velocity profile of a potential or free vortex. Also, the method of determining potential vortex surface deflection at steady state using the approach of superimposing analytically generated curves on photographic images of the actual surface proved very reliable. Also, determining potential vortex surface velocity using video that recorded the time required for a red-spotted Styrofoam ball to orbit the basin at a measured distance from the central rotating core also proved very useful.

FIG. 11. Methods presented are successful for predicting transient properties of the potential vortex.

In addition, it is proved that for concentric cylinders where the inner cylinder rotates and the outer cylinder is stationary the potential flow equations are not sufficient for the prediction of potential vortex shape and velocity profile when $r_1/r_0 < 5$. Therefore, a cylinder separation ratio greater than $r_1/r_0 = 5$ is considered necessary for generating a potential vortex under laboratory conditions. However, surface velocity measurements in

areas sufficiently far away from the inner rotating surface and outer stationary surface were accurate compared to theoretical prediction using the general derivation of fluid flow between two concentric cylinders. Agreement between theoretical potential vortex predictions and experimental results were limited due to severe flow separation from the inner rotating boundary and viscous interference from the outer stationary cylinder. As stated previously, the presence of an outer cylinder greatly affects prediction of potential vortex surface deflection and velocity. However, these results also show that surface deflection predictions apply equally when the cylinder is located infinitely far away or a finite distance away but depart greatly from measurement near the central rotating cylinder where turbulence and flow separation are most intense. Also, the transient solution of the Navier-Stokes equation (Eqn. 26) for concentric cylinders converges to inviscid flow results because at steady state the energy-momentum into a fluid volume equals the energy-momentum out of a fluid volume balancing the viscous effects of fluid motion. This relationship is clearly shown by the Bernoulli equation that includes kinetic and potential energy and by the associated Navier-Stokes equation that provides the friction terms required for conservation of energy-momentum at steady state. Finally this work can be applied to the measurement of the vortex flow generated by aircraft wing tips, aircraft jet engines and atmospheric phenomena like tornadoes and hurricanes where physical measurements are impractical or impossible.

References

[1] F. M. White, *Fluid Mechanics*, (McGraw-Hill, New York, 2010)

[2] F. P. Beer and E. R. Johnston, *Vector Mechanics for Engineers* (McGraw-Hill, New York, 1970)

[3] F. M. White, *Viscous Fluid Flow*, (McGraw-Hill, New York, 2005)

[4] H. Schlichting, *Boundary Layer Theory*, p. 87-89 (McGraw-Hill, New York, 1979)

[5] J. Cipolla, "Solid Vortex Transient Velocity and Free Surface Shape", ME Design Project, URI (1972)

[6] R. C. Lessmann, "Diffusion of a Rectangular Vortex in a Weakly Viscoelastic Liquid", J. Hydronautics, VOL. 4, NO. 4 (1970)

[7] D. Halliday, R. Resnick, J. Walker, *Fundamentals of Physics-7th Edition*, p. 330-348 (John Wiley & Sons, New Jersey, 2005)

[8] M.C. Wendl, "General Solution for the Couette Flow Profile", Physical Review E **60**, 6192–6194 (1999)